



Article

Optimization of the Liquid Desiccant Cooling Systems in Hot and Humid Areas

Yanling Zhang ^{1,2,*} , Hao Zhang ¹, Hongxing Yang ², Yi Chen ^{3,*}  and Chun Wah Leung ¹

¹ School of Professional Education and Executive Development, The Hong Kong Polytechnic University, Hong Kong, China

² Renewable Energy Research Group, Department of Building Environment and Energy Engineering, The Hong Kong Polytechnic University, Hong Kong, China

³ College of Marine Equipment and Mechanical Engineering, Jimei University, Xiamen 361021, China

* Correspondence: yanling.zhang@connect.polyu.hk (Y.Z.); chenyi0511@jmu.edu.cn (Y.C.)

Abstract: Air-conditioning systems in hot and humid regions account for over 50% of total energy usage. Integrating an indirect evaporative cooling (*IEC*) and a liquid desiccant dehumidifier (*LDD*) as the liquid desiccant cooling system (*LDCS*) presents an energy-saving and emission-reducing solution to replace traditional mechanical vapor compression refrigeration (*MVCR*) systems. This integration overcomes the regional limitations of *IEC* in hot and humid areas. The newly developed *LDCS* uses exhaust air as the working air source and solar energy as the heat source for desiccant solution regeneration. This study aims to develop an empirical model for the outlet parameters of the *LDCS*, propose an optimization strategy for its operating parameters, and assess the potential and energy performance through parameter analysis and multifactor optimization. By conducting sensitivity analysis and optimizing six critical parameters based on a response surface model (*RSM*), the system outlet temperature, relative humidity, and coefficient of performance (*COP*) are improved as the optimization objectives. The regional capability is demonstrated in three selected hot and humid cities. The results indicate that the *LDCS* can significantly increase the *COP* by 57.3%. Additionally, it can meet the dehumidification demand when operating with 25% of the air extracted in the *RIEC* during months with high humidity and temperature. This study will facilitate the application of *IEC* and *LDD* technologies, guide the design and operation scheme of the system, and promote energy-saving and emission-reducing solutions in hot and humid regions.

Keywords: liquid desiccant dehumidification; indirect evaporative cooling; multi-parameter analysis; multi-objective optimization



Citation: Zhang, Y.; Zhang, H.; Yang, H.; Chen, Y.; Leung, C.W.

Optimization of the Liquid Desiccant Cooling Systems in Hot and Humid Areas. *Sustainability* **2023**, *15*, 13511.

<https://doi.org/10.3390/su151813511>

su151813511

Academic Editor: Kian Jon Chua

Received: 30 July 2023

Revised: 4 September 2023

Accepted: 7 September 2023

Published: 9 September 2023



Copyright: © 2023 by the authors. Licensee MDPI, Basel, Switzerland. This article is an open access article distributed under the terms and conditions of the Creative Commons Attribution (CC BY) license (<https://creativecommons.org/licenses/by/4.0/>).

1. Introduction

Air conditioning systems are increasingly becoming energy-intensive and are predicted to be the second-largest source of electricity consumption in the next three decades [1,2]. In hot and humid regions, traditional mechanical vapor compression refrigeration systems (*MVCR*) consume over 50% of the building's total energy use and have a limited coefficient of performance (*COP*) [3]. This poses challenges for cooling and dehumidification in high-humidity regions [4]. To address these issues, researchers are exploring safe and efficient alternatives to traditional *MVCR* systems, such as indirect evaporative cooling (*IEC*) and liquid desiccant dehumidification (*LDD*) [5] technologies. The combination of *LDD* and *IEC* technologies in a regenerative internally cooled liquid desiccant air conditioning system (*RLDAC*) has shown great promise in overcoming the limitations of traditional air conditioning systems.

The liquid desiccant cooling system (*LDCS*) represents a promising technology for achieving energy-efficient and environmentally friendly air conditioning. However, the application of its two main components, the *IEC* and *LDD* is constrained by regional climate conditions. On the one hand, *IEC* has demonstrated significant cooling potential

in dry and cold regions [6]. However, in humid areas characterized by elevated wet bulb temperatures, *IEC* encounters limitations in providing adequate evaporative cooling capacity [6]. Its condensation method is not enough to achieve the dehumidification goal [7]. Chu et al. [8] found that the heat transfer performance of a regenerative indirect evaporative cooler (*RIEC*) is not prominent in wet areas. On the other hand, the reduced vapor pressure difference of *LDD* at high temperatures compromises its dehumidification efficacy [9]. To overcome these limitations, previous studies have attempted to integrate *IEC* and *LDD*. Zhang et al. [10] developed a device that combines *IEC* and *LDD*. Although this device increased the dry bulb efficiency by 39%, the currently available device is insufficient to replace energy-efficient air conditioners in providing an air-conditioned air supply. Therefore, simply integrating *LDD* and *IEC* is not enough to achieve the target supply air temperature and moisture content [11] in hot and humid regions. It is crucial to explore the performance of liquid desiccant cooling systems and their applicability in hot and humid regions.

The purpose of a regional applicability study is to assess the cooling and dehumidification capabilities for conditioning air to target operating conditions, as well as to evaluate its energy consumption and heat transfer performance. Previous studies [10,11] have demonstrated that certain liquid desiccant cooling systems may struggle to consistently provide low-temperature and dry air, particularly in hot and humid regions. To address this challenge, it becomes imperative to configure and optimize system parameters according to varying climatic conditions. It is important to configure the system to make it handle the air to meet the air conditioning supply conditions. In previous multi-stage evaporative cooling and dehumidification systems, dehumidification devices represented by desiccant wheels [12], liquid desiccants [5,13], and evaporative coolers [14] were often used as air pretreatment or recovery devices. It is rare to use a multi-stage *LDAC* system directly to treat the air to the supply air state point without any vapor compression device. In prior studies on *LDD* – *IEC* [15,16], some *LDD*-assisted cooling methods relied on coils [16], or they involved pre-cooling procedures [15]. In the newly proposed system, the regenerative *IEC* employs a portion of the low-temperature supply air as the air source for the indirect cooling channels. The *LDD* uses waste heat recovered from the exhaust air as a source of internal cooling air.

The existing study on systems integrating *LDD* and *IEC* has faced challenges in optimizing configurations to resolve the trade-off between system air handling performance and energy efficiency. On one hand, integrated systems may require higher resource consumption to condition air to the desired specifications [17]. Heidarinejad et al. [18] developed a multi-stage system using *IEC* and directly evaporative cooling that achieved better cooling performance, but it resulted in a 55% increase in water consumption compared to *MVCRs*. Kim et al. [16] developed a multi-stage system using *LDD*, *IEC*, and *DEC* that avoided the use of vapor compression devices. However, the excessively complex design of this system resulted in a significantly higher initial investment cost. Consequently, striking a balance between the cooling and dehumidification capabilities of the system and its energy performance has emerged as a critical challenge. On the other hand, there are cross-effects between the parameters that affect the system's performance. Ren et al. [19] used *RSM* to optimize a desiccant wheel cooling system and found that many factors had cross effects on the system's performance indicators. Hu [20] tested the dehumidification capabilities of *LDD* in different climatic zones in China and found that *LDD* had varying sensitivities to changes in solution concentration in different cities. Hence, there is a compelling need for a comprehensive optimization approach that considers multiple parameters and objectives to effectively balance the system cooling and dehumidification capabilities with its energy performance.

In summary, it is necessary to develop a new system configuration with improved cooling and dehumidification performance and conduct regional adaptability studies in order to achieve the cooling and dehumidification goals in humid regions [21,22]. In the newly proposed system, the regenerative *IEC* uses a portion of the low-temperature supply

air as the air source for the indirect cooling channels. *LDD* uses waste heat recovered from the exhaust air as a source of internal cooling air and the liquid desiccant regenerated by the solar heat collector. Through sensitivity analysis, key components and parameters of the system have been identified, and empirical formulas have been generated using statistical methods to predict the performance of the liquid desiccant cooling system (*LDCS*) and optimize six key parameters, namely temperature, relative humidity, inlet air velocity, desiccant concentration, return air ratio, and number of transfer units. Furthermore, the regional adaptability of the *LDCS* system in humid regions is explored, with the system performance coefficient (*COP*) as well as the outlet temperature and humidity being optimized targets.

2. System Modeling

2.1. Proposed System

Figure 1 depicts the proposed schematic diagram for the *LDCS*, which consists of internally cooled *LDD* assisted by solar energy regeneration and *RIEC*. The system is designed to address the heat and humidity load by dehumidifying the fresh air first in the *LDD* unit, followed by cooling the air with *RIEC* before circulating it throughout the room. To ensure the efficient operation of the *LDD*, the working air for internal cooling is drawn from the indoor exhaust air. The liquid desiccant cooling system has three loops, including the solar regenerator solution and dehumidifier loop, the internal evaporative cooling water loop, and the fresh air loop.

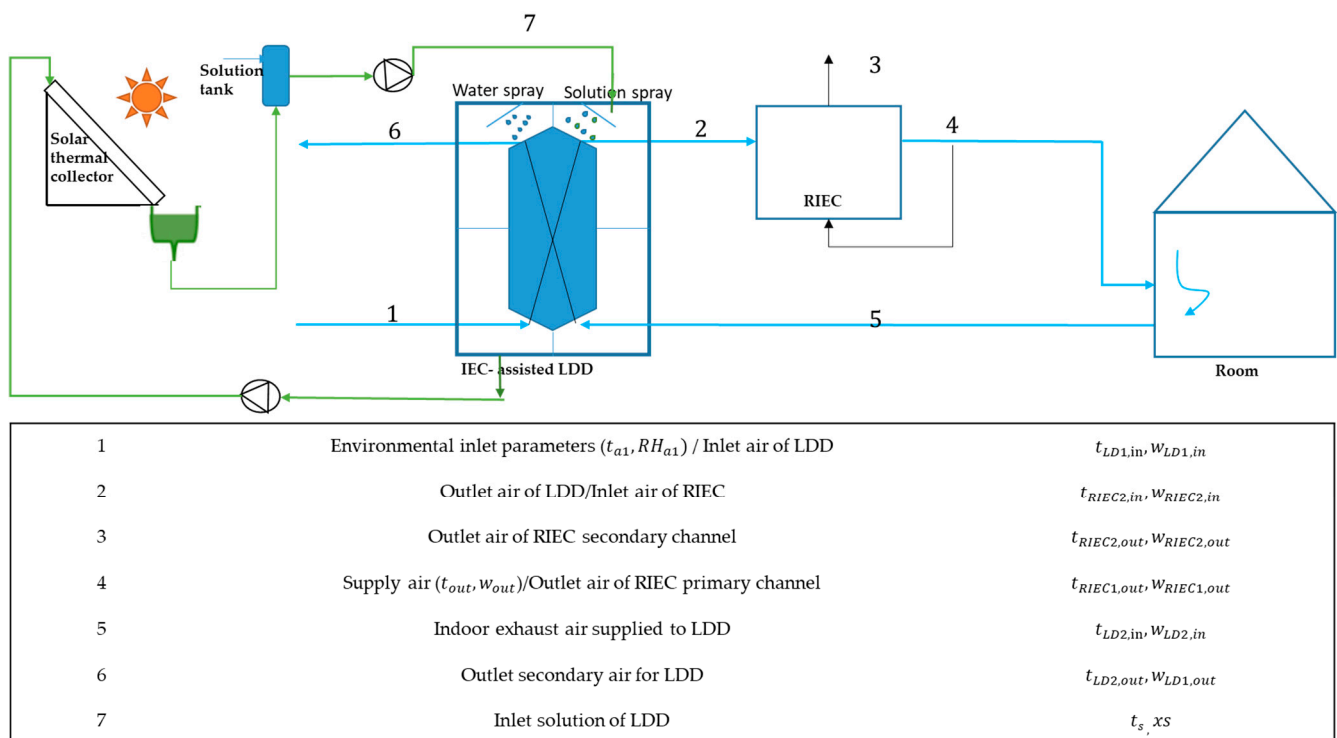


Figure 1. Schematic diagram of liquid desiccant cooling system.

The main components of the system, *LDD* and *RIEC*, are modeled separately. Figure 2 presents the flow chart of system model creation. The model of the system makes the following assumptions: 1. The system unit is adiabatic, meaning that there is no exchange of heat with the environment and no air leakage. 2. The thermal properties of water are consistent. 3. The water film and liquid desiccant equally cover the wall. 4. The Lewis number remains constant on the water and solution surfaces. 5. The solar thermal collector can provide enough heat for the solution regeneration process.

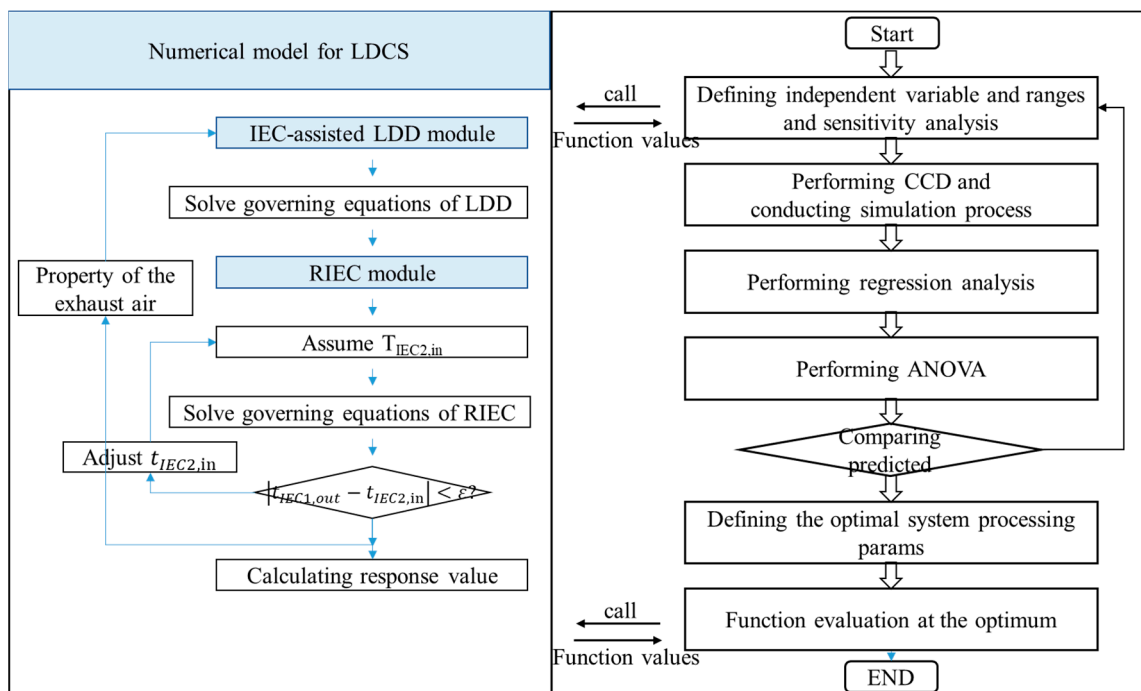


Figure 2. Flowchart of the optimization process of the LDCS.

2.2. Numerical Model of the LDD and RIEC

The establishment of the mathematical model for the system primarily relies on the heat and mass transfer processes of desiccation and evaporative cooling that occur in two key heat exchangers. Equations (1)–(10) constitute the governing equations and their solutions for primary and secondary airflows in the LDD. Equations (11)–(13) constitute the control equations for RIEC without considering condensation.

A two-dimensional finite model was built to simulate the dehumidification and internal evaporative cooling process of LDD. NTU represents the number of heat transfer units in the dehumidification channel of LDD ($NTU = \frac{\alpha_{LD1} \cdot A_{wall}}{m_{LD1} \cdot c_{p,a1}}$). In the process of heat mass transfer between solution and air, the Lewis number ($Le = \frac{\alpha_{LD1}}{\alpha_{mLD1} \cdot c_{p,a1}}$) in LDD and RIEC is taken as 1 [23], the number of mass transfer units in the primary channel of LDD can be expressed as $NTU_m = \frac{\alpha_{ms} \cdot A_{wall}}{m_{a1}}$.

Equations (1) and (2) can express the latent and sensible heat processes in the microelements in the dehumidification channel.

$$dQ_{sen,s} = \alpha_{LD1}(t_s - t_{LD1,in})2A \frac{dx}{l} \quad (1)$$

$$dQ_{lat,s} = \frac{\alpha_{LD1}}{c_{p,a1}} \cdot r_w \cdot (w_s - w_{LD1})2A \frac{dy}{l} \quad (2)$$

The calculation of the constant pressure-specific heat of humid air involves the summation of the constant pressure-specific heat of dry air and water vapor, expressed as $c_p = c_{pg} + c_{pv}$. The energy and mass conservation equations for LDD primary channels are presented in Equations (3) and (4), while Equations (5) and (6) depict the corresponding equations for the secondary channels. The heat transfer between the two channels can be expressed as Equation (7).

$$Qdx + m_{LD1,in}dh_{LD1,in} - dm_s c_{ps} t_s = 0 \quad (3)$$

$$m_{LD1,in}dw_{LD1,in} = dm_s \quad (4)$$

$$-Qdy + m_{LD2,in}dh_{LD2,in} - dm_w c_{pw} t_w = 0 \quad (5)$$

$$m_{LD2,in}dw_{LD2,in} = dm_w \quad (6)$$

$$Q = K(t_s - t_w)d_x dy \quad (7)$$

where the enthalpy value of humid air can be expressed as the function of air temperature and moisture content: $h = c_{pg}t + (2500 + c_{pvd})d$, $c_p = c_{pg} + c_{pvd}$.

The product air channel and the internal cooling channel in the RIEC model were built as two-dimensional finite models. The heat and mass balances, as well as the mechanisms of heat and mass transfer for both the primary (Equation (10)) and secondary channels (Equations (8) and (9)), are solved under the assumption that the incoming air undergoes appropriate latent heat treatment before entering the RIEC. Equations (11) and (12) display the energy balance equation of the control volume and the mass balance of the evaporation film in the secondary channel.

$$\alpha_{RIEC2}(t_{wall} - t_{RIEC2,in})2A\frac{dy}{l} = c_{pRIEC2,in}m_{RIEC2,in}dt_{RIEC2,in} \quad (8)$$

$$\alpha m_{RIEC2}(\omega_{t_{wall}} - \omega_{RIEC2,in})2A\frac{dy}{l} = m_{RIEC2,in}dw_{RIEC2,in} \quad (9)$$

$$\alpha_{RIEC1}(t_{RIEC1,in} - t_{wall})2A\frac{dx}{l} = c_{pRIEC1,in}m_{RIEC1,in}dt_{RIEC1,in} \quad (10)$$

$$dm_{ew} = m_{RIEC1,in}dw_{RIEC1,in} \quad (11)$$

$$m_{RIEC1,in}dh_{RIEC1,in} - c_{pRIEC1,in}m_{RIEC1,in}dt_{RIEC1,in} = d(cp_{wall}t_{ew}m_{ew}) \quad (12)$$

The return air ratio of LDD (RC) is the air mass flow ratio between the internal cooling and dehumidification channels in the LDD. ($RC = \frac{m_{RIEC1,out}}{m_{LD1,in}}$). The air mass flow relationship between the fresh air sent into the room by the RIEC and the exhaust air entering the LDD depends on the extraction ratio (re) of RIEC. Assuming that the indoor air pressure remains constant, the air mass flow relationship between RIEC and LDD secondary channel depends on the extraction ratio (re) of RIEC ($re = 1 - RC$).

$$m_{RIEC1,out} = (1 - re) \cdot m_{LD1,in} \quad (13)$$

The aforementioned control equations can be written as standard ordinary differential equations. Using the finite difference method (FDM) to discretize the differential terms into algebraic forms, numerical simulation results at each discretized node can be obtained by simultaneously solving a set of algebraic equations.

2.3. Model Validation

The accuracy of the numerical models developed for the main components of LDAC (LDD and RIEC) have been validated by two published research papers (Figure 3). The simulation results of the internally cooled LDD are compared to a study that used the IEC as its internal cooling method. To explore the exit moisture content of primary air produced by an internally cooled LDD process at various mass flow rates, the numerical model created by Saman and Alizadeh [24] was compared with the new model. The output moisture content parameters of the two models were compared under identical primary and secondary air intake conditions and operating circumstances (primary air: 33 °C, 0.171 kg/kg; secondary air 27 °C, 0.100 kg/kg, $m_{LD1} = 0.42$ kg/s, $v_{LD1} = 1$ m/s, $RC = 1$).

The results of the newly constructed model varied from those in the literature by 1.5 to 6.3%. Riangvilaikul and Kumar [25] conducted experiments using partially treated primary air directly as the secondary air source in the *RIEC* model. The outlet temperature is examined in this experiment. The previous model was applied to the current study, simulating it with the same inlet condition and flow pattern. The outlet temperature differential ranged from 0.9% to 10.0% based on the statistical analysis.

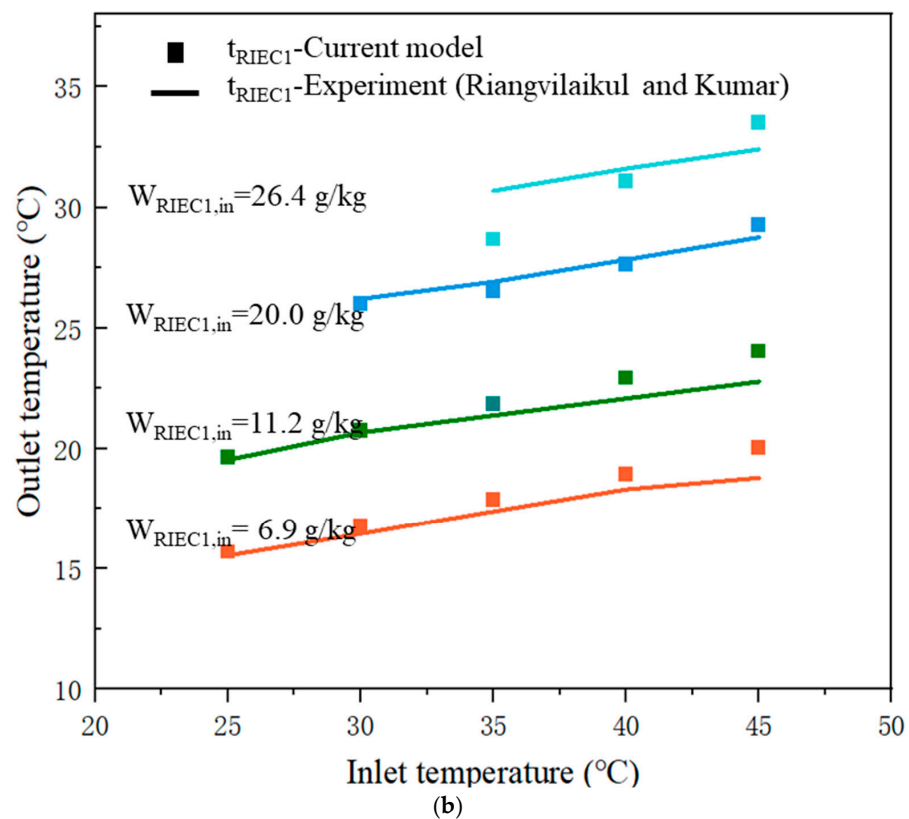
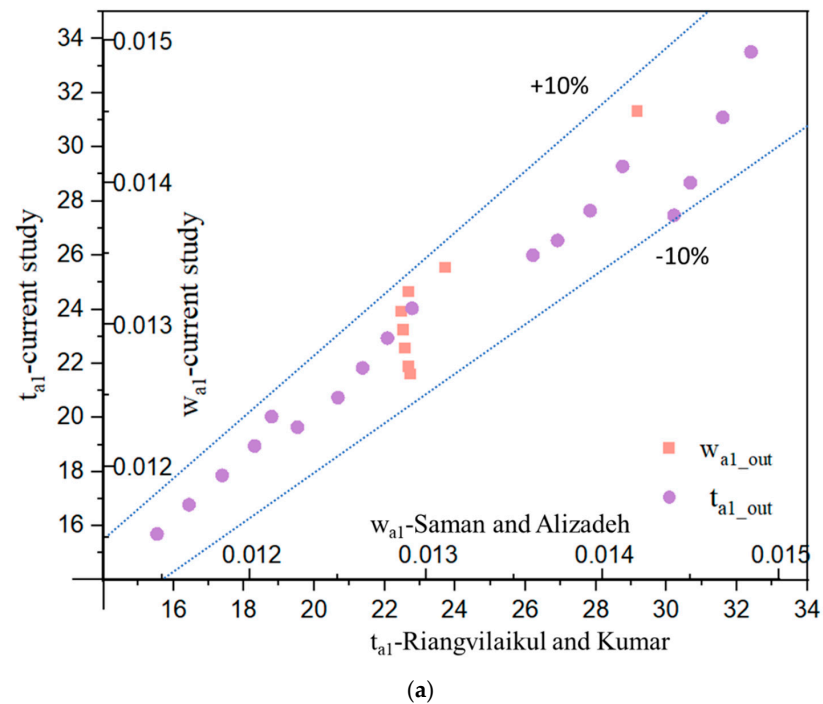


Figure 3. Cont.

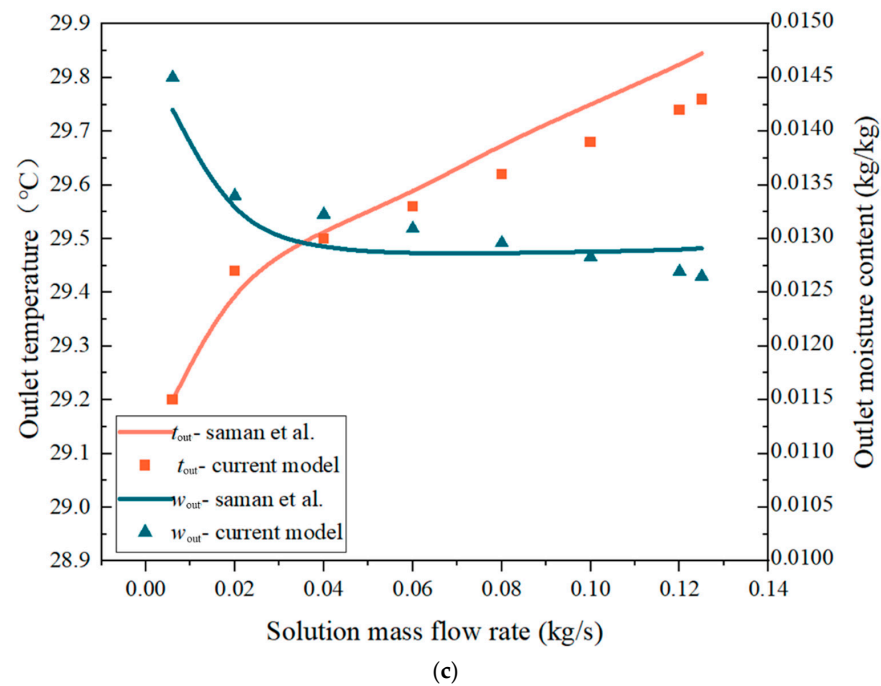


Figure 3. (a) Validation of the LDD and RIEC numeric models [24]. (b) Comparison of RIEC experimental results with published simulation model for model validation [25]. (c) Comparison of LDD simulation results with published simulation model for model validation [24].

Based on the above comparative experiments on RIEC [25] and simulations on LDD with internal indirect evaporative cooling [24], the numerical model comparison findings indicate deviations between anticipated values and experimental data ranging from 2.4% to 16.3%. The present model is capable of forecasting outlet temperature and humidity for both LDD and RIEC models with an acceptable discrepancy between created models and reported data.

2.4. Evaluation Indicators

Equation (14) was used to calculate the coefficient of performance (COP), which was employed as the assessment index.

$$COP = \frac{Q_{sen} + Q_{lat}}{W_{fans} + W_{pumps}} \quad (14)$$

The energy-consuming components in the system include solution pumps, a water pump, and two fans, which can be calculated according to Equations (15) and (16).

$$W_{pump} = m_w \cdot g \cdot H_{pump} \cdot K_{pump} \quad (15)$$

$$W_{fan} = \frac{L \cdot P_{fan}}{3600 \cdot 1000 \cdot \eta_0 \cdot \eta_1} \quad (16)$$

where P is the full wind pressure of the fan, Pa; L is the air volume, m^3/h ; H_{pump} is the pump head, m; η_0 is the internal efficiency of the fan, which is 0.75, η_1 is the mechanical efficiency, which is assumed to be 0.95; K_{pump} is the motor capacity factor and is supposed to be 1.15 [1].

3. Empirical Model and Multi-Objective Parameter Optimization

The optimization within this system aims to identify the optimal combination of system parameters to achieve the dual objectives of air dehumidification and cooling

while simultaneously maximizing the *COP*. Six key parameters have been selected for sensitivity analysis to assess the performance of the *LDCS* across diverse environmental and operational conditions. The central composite design (*CCD*) is a statistical design technique widely employed in research and engineering to examine how a system or process responds to multiple factors, accounting for both linear and nonlinear effects, as well as potential interactions among these factors. In this study, *CCD* is utilized to determine representative combinations of multiple factors. These representative cases effectively represent the test results of all variable parameter combinations.

In the system, six key parameters (primary air temperature t_{a1} , primary air relative humidity RH_{a1} , solution concentration x_s , primary-to-secondary airflow ratio RC , primary air velocity v_{a1} , and the number of transfer units NTU) were selected for sensitivity analysis to identify the parameters that exert a substantial influence on the *COP* of *LDCS*. Following the sensitivity analysis, independent variables (t_{a1} , w_{a1} , RC , v_{a1} , x_s) that had a significant impact on the response value were selected, and a 50-group test design with three levels for each parameter was carried out. The specific values for each parameter are detailed in Table 1. The temperature and relative humidity ranges are selected based on the weather conditions in hot and humid regions. The recommended air velocity for *IEC* or *LDD* typically falls within the range of 1 to 3 m/s. The concentration of the solution is chosen within the solubility range of *LiCl* [26]. The simulations were conducted according to the arrangement specified by the *CCD*, resulting in a total of 50 tests. The analysis of the test results was carried out utilizing the Design Expert version 13.0.

Table 1. The values range for each parameter in *LDCS*.

Name	t_{a1}	w_{a1}	v_{a1}	x_s	RC
Units	°C	kg/kg	m/s	%	%
level 1	24	60	1	0.3	0.5
level 2	32	70	2	0.4	0.7
level 3	40	80	3	0.5	0.9

The sensitivity analysis explores the main effects of the parameters, and the interaction effects of the parameters can be further explored. Moreover, 50 *LDCS* simulated data were analyzed by analysis of variance (*ANOVA*) to identify the significant parameters influencing three evaluation criteria: t_{out} , w_{out} , and *COP*. The *p*-value is calculated to assess the probability of obtaining a test statistic as extreme as or more extreme than the observed statistic under the assumption that the null hypothesis is true. A lower *p*-value indicates stronger evidence against the null hypothesis. A response surface model is constructed using the obtained data, and its statistical significance is evaluated using an F-test at a 95% confidence level [22,27]. A *p*-value less than 0.05 is considered evidence that the regression model is capable of predicting the response for the parameters that significantly affect the system performance; a curve fitting is employed to establish an empirical mathematical model. To assess the relationships between the responses and validate the empirical model, correlation coefficients of determination (R^2) were used. Taking the outlet temperature (t_{out}), humidity (w_{out}), and *COP* of the product air as optimization objectives, the impact of parameter variations on system performance is analyzed using the *DFA*, and multi-objective optimization is conducted.

The flowchart of the optimization process is shown in Figure 3. The system optimization process includes the establishment of mathematical models, regression analysis, sensitivity analysis of single values and cross-effect parameters, and multi-objective optimization. The numerical model developed in the previous section provides data for fitting the empirical model. Sensitivity analysis is first used to explore the effect of single-valued variables on the air outlet status and *COP* performance of the system (Table 2). The central composite design (*CCD*) consists of a square grid with four additional test points located at the corners, in the center, and along the axial directions. It is widely used for fitting

second-order surface equations. A regression equation based on a second-order polynomial model (Equation (17)) can describe the relationship between the response and the terms in the model and characterize this response surface algebraically. The fitted response surface model was statistically analyzed by analysis of variance (ANOVA). The significance of each additional term is evaluated in sequence using the F-test. The results of the ANOVA allow the identification of first-order terms, intersection terms, and higher-order terms that have a significant impact on outlet air performance and *COP*.

Table 2. Parameter range for the sensitivity analysis of the six parameters.

Parameters	Basic Scenario	−30%	−10%	1	+10%	+30%
t_{a1} (°C)	33	23.1	29.7	33	36.3	42.9
RH_{a1} (%)	70	49	63	70	77	91
v_{a1} (m/s)	2	1.4	1.8	2	2.2	2.6
x_s	0.35	0.245	0.315	0.35	0.385	0.455
<i>RC</i>	0.7	0.49	0.63	0.7	0.77	0.91
<i>NTU</i>	4	2.8	3.6	4	4.4	5.2

Therefore, based on a second-order polynomial model, a multivariate regression analysis using statistical methods is performed on the three optimization objectives (t_{out} , w_{out} , *COP*) and five parameters to generate empirical equations. The desirability function approach (*DFA*) is used for multi-objective optimization of the three optimization objectives (Equations (18) and (19)).

Given the substantial variations in specific meteorological conditions across different cities within hot and humid regions, there exists a multitude of scenarios encompassing hot and humid weather conditions that necessitate exploration. Tailored optimization strategies are believed to be invaluable in addressing these diverse scenarios. The combined effects of meteorological and operating parameters can be used to explore the optimal operation of the system under different weather conditions. Air velocity, *RC*, and solution concentration were identified as parameters that primarily affected system performance, and cross-effects between operating parameters significantly influenced the variation in *COP*. Therefore, modifying operational parameters through cross-interaction holds the potential to enhance overall system performance. Finally, the performance of the operation scheme under different meteorological conditions is explored to explore the regional applicability of the system. Three cities (San Juan, Kuala Lumpur, and Hong Kong) have been selected for case studies with varying temperature and moisture content (Table 3) to explore the performance of the system in hot and humid regions. The intake conditions are chosen based on the local annual extreme design conditions [28]. The optimization of operational parameters, as outlined in Table 3, and the prediction of target values have been conducted for these three cities.

$$y = \alpha_0 + \sum_{i=1}^j \alpha_i x_i + \sum_{i=1}^k \alpha_{ii} x_i^2 + \sum_{i=1}^{i < j} \alpha_{ij} x_i x_j \quad (17)$$

$$d = \left(\frac{y - l}{T - l} \right)^r, \quad L \geq y \geq T \quad (18)$$

$$D = (d_1 d_2 \cdots d_n)^{\frac{1}{n}} \quad (19)$$

Table 3. Design meteorological parameters and optimized parameters of the cities.

Extreme Annual Design Conditions			Optimized Parameters		
City	T (°C)	RH (%)	v_{a1} (m/s)	x_s -	RC -
Kuala Lumpur	34.1	86.7	2.3	0.4	0.75
San Juan	34.5	68.4	2.3	0.4	0.7
Hong Kong	33.7	74.3	2	0.4	0.7

4. Results

The results of the multifactor analysis of variance are provided to identify the key parameters that affect the system *COP*. Subsequently, empirical equations are fitted based on the key parameters to predict the system's outlet parameters (t_{out} , w_{out}) and *COP*. A two-factor analysis is then conducted on these empirical equations to establish a ranking of the factors and evaluate their significance in shaping the *COP*. Finally, the optimization scheme and the findings pertaining to the regional applicability of the *LDCS* are presented.

4.1. Empirical Model of Performance Indicators

The empirical correlations of the predicted *COP* efficiency and supply air temperature and humidity values for the internally cooled liquid desiccant cooling system were derived as functions of the six operating parameters based on the numerical model. Statistical analysis was conducted using regression analysis and analysis of variance (ANOVA).

The results of the variance analysis revealed the noteworthy impact of operational parameters and their interactions with two factors on the performance of outlet air supply and *COP*. For the *COP* of the *LDCS* system, all operational and design parameters showed high significance (p -value < 0.05), while only some cross-term operational parameters exhibited significance to the target values. For example, the interaction of inlet air temperature and airflow velocity showed high significance for *COP*, while the interaction of inlet air relative humidity and airflow velocity displayed low significance for the outlet air temperature of the system (p -value > 0.10). The combined effects of meteorological and operational parameters can be utilized to explore the optimized operation of the system under different weather conditions. As discussed in the preceding section, the cross-interactions among operational parameters, including airflow velocity, *RC*, and solution concentration significantly influenced *COP* variations. Therefore, modifying operational parameters with cross-interactions can lead to improved system performance. Consequently, the parameters deemed significantly important for *LDCS* metrics, along with their interactions, were selected to formulate empirical correlations aimed at predicting the system's product air outlet conditions and the *COP* of the *LDCS*.

The empirical correlations for the product air temperature, humidity content, and *COP* of the *LDCS* system are shown in Equations (20)–(22). The R^2 values of the proposed model were found to be 98.6% for the product air temperature, 98.7% for the outlet humidity content, and 98.4% for *COP*, indicating a good agreement between the simplified empirical formula predictions and the numerical model data.

$$\begin{aligned}
 COP = & 44.3285 - 1.9296 * t_{a1} - 0.3650 * RH_{a1} - 4.2330 * v_{a1} + 17.7689 * x_s - 24.2765 * RC + 0.0082 \\
 & * t_{a1} * RH_{a1} + 0.1376 * t_{a1} * v_{a1} - 0.2871 * t_{a1} * x_s + 0.6828 * t_{a1} * RC + 0.0221 * RH_{a1} \\
 & * v_{a1} - 0.0749 * RH_{a1} * x_s + 0.1152 * RH_{a1} * RC - 0.9795 * v_{a1} * x_s + 1.4046 * v_{a1} * RC \\
 & + 4.5697 * x_s * RC + 0.0180 * t_{a1}^2 + 0.0005 * RH_{a1}^2 - 0.2878 * v_{a1}^2 - 1.3211 * x_s^2 - 2.5112 \\
 & * RC^2
 \end{aligned} \quad (20)$$

$$\begin{aligned}
t_{out} = 25.3378 & + 0.0616 * t_{a1} + 0.0028 * RH_{a1} - 3.5461 * v_{a1} - 0.0582 * x_s - 12.8983 * RC - 3.125e^{-6} \\
& * t_{a1} * RH_{a1} + 0.00023 * t_{a1} * v_{a1} - 0.00253 * t_{a1} * RC + 6.8749e^{-6} * RH_{a1} * v_{a1} \\
& + 0.00032 * RH_{a1} * x_s - 0.00067 * RH_{a1} * RC + 0.00356 * v_{a1} * x_s + 1.9604 * v_{a1} * RC \\
& + 0.0534 * x_s * RC - 0.00091 * t_{a1}^2 - 1.6895e^{-5} * RH_{a1}^2 + 0.0653 * v_{a1}^2 - 0.0820 * x_s^2 \\
& + 10.1304 * RC^2
\end{aligned} \quad (21)$$

$$\begin{aligned}
w_{out} = -0.0063 & + 0.000575 * t_{a1} + 0.00027 * RH_{a1} + 0.001909 * v_{a1} - 0.063808 * x_s - 0.000279 \\
& * RC - 2.1625e^{-6} * t_{a1} * RH_{a1} + 3.249e^{-06} * t_{a1} * v_{a1} + 0.0007925 * t_{a1} * x_s - 5.6250e^{-6} \\
& * t_{a1} * RC + 3.374e^{-6} * RH_{a1} * v_{a1} + 0.000207 * RH_{a1} * x_s - 1.750e^{-6} * RH_{a1} * RC \\
& + 0.0053075 * v_{a1} * x_s - 0.0001238 * v_{a1} * RC + 9.374e^{-05} * x_s * RC - 5.0585e^{-6} * t_{a1}^2 \\
& - 1.2685e^{-6} * RH_{a1}^2 - 0.000618 * v_{a1}^2 + 0.00432 * x_s^2 + 0.000469 * RC^2
\end{aligned} \quad (22)$$

4.2. Parameter Analysis

4.2.1. Single-Value Factor Analysis

Identifying the effect of variations in single-value parameters on the system's robustness is imperative for optimizing its performance. Based on the single-value parameter analysis discussed in the previous section, sensitivity analysis is conducted for the six parameters that significantly affect the system-optimized objectives (Figure 4a). The impact of each parameter is examined by deviating $\pm 10\%$ and $\pm 30\%$ to assess their influence on the performance (Table 2). The base scenario is represented by the gray line, with the selection of temperature and humidity values based on meteorological data from a hot and humid city. The operating parameters are referenced from recommended values in previous studies on LDD and IEC performance.

Analyzing and understanding the behavior of the system within and outside these regions are essential for evaluating its overall performance and identifying factors that contribute to its efficiency. By comparing the performance with the baseline scenario, the impact of different operational parameters, environmental conditions, or design modifications on the system's effectiveness can be explored.

Figure 4a,b illustrates the impact of parameter variations on COP based on the baseline scenario. The inlet temperature has the greatest influence on the system COP; it is determined by the outdoor environmental conditions. However, without changing the operating parameters, it is not possible to improve the system COP under constant outdoor conditions. The factor v_{a1} and RC have a significant impact on the system COP. RC determines the ratio of the secondary airflow in IEC and LDD, allocating the cooling and dehumidification capacity of the system. It can significantly affect the system's COP and has greater potential for system optimization.

The solution concentration and airflow velocity are significant operating parameters that affect the outlet humidity and temperature. These parameters have a substantial impact on the system's performance and energy efficiency and require further optimization. Figure 4c,d illustrate the influence of altering six parameters on the outlet air temperature and moisture content, using the baseline scenario as a reference. The gray circles represent the temperature and humidity differences at the outlet of the system in the basic scenario. The points outside the circles represent the increase in the difference between the inlet and outlet temperature and humidity of the system after changing the corresponding parameters. The dots in the circles indicate that changing the value of the corresponding parameter results in a smaller change in temperature and humidity at the inlet and outlet of the system than in the baseline scenario. The results indicate a relatively balanced influence of the six parameters on the change in moisture content of the outlet air. Among them, airflow velocity and solution concentration, as operational parameters, exhibit a significant effect on the moisture content. Decreasing the airflow velocity by 30% leads to an additional removal of 1.769 g/kg of water vapor compared to the baseline scenario. Moreover, the outdoor temperature also affects the dehumidification performance of the system under the

same relative humidity conditions, indicating the system's sensitivity to high-temperature and high-humidity environments.

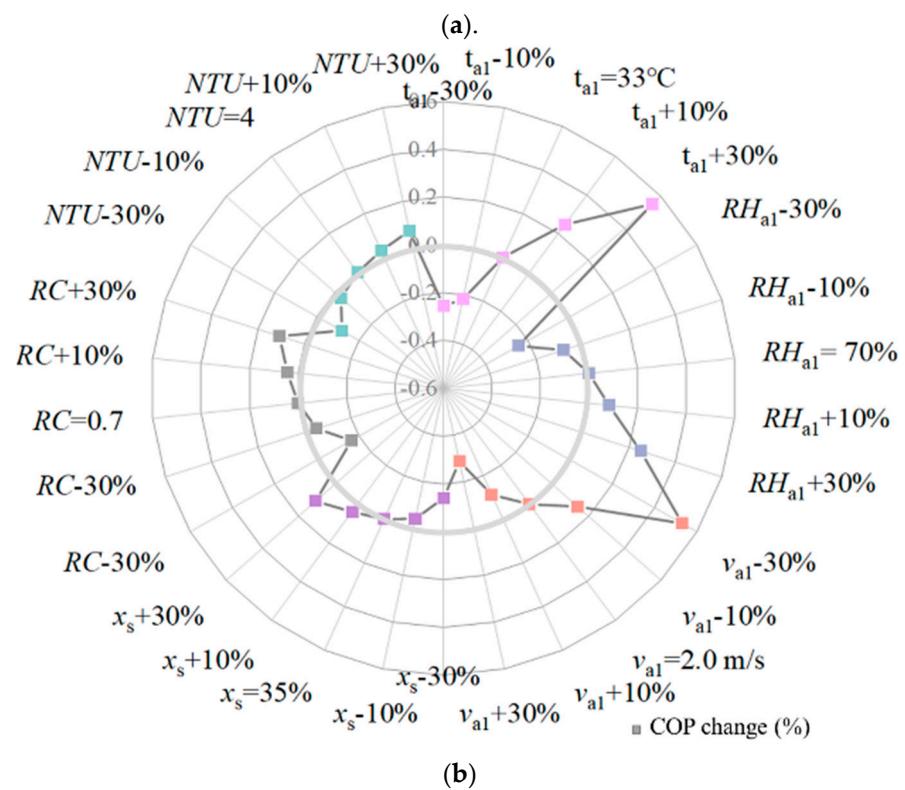
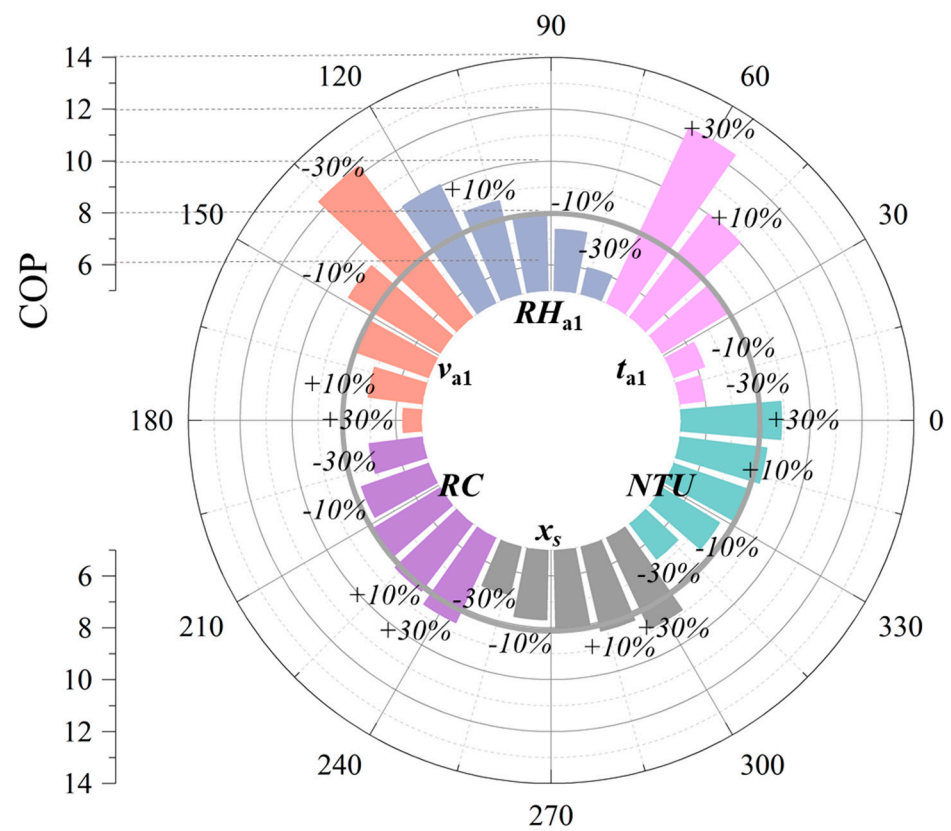


Figure 4. Cont.

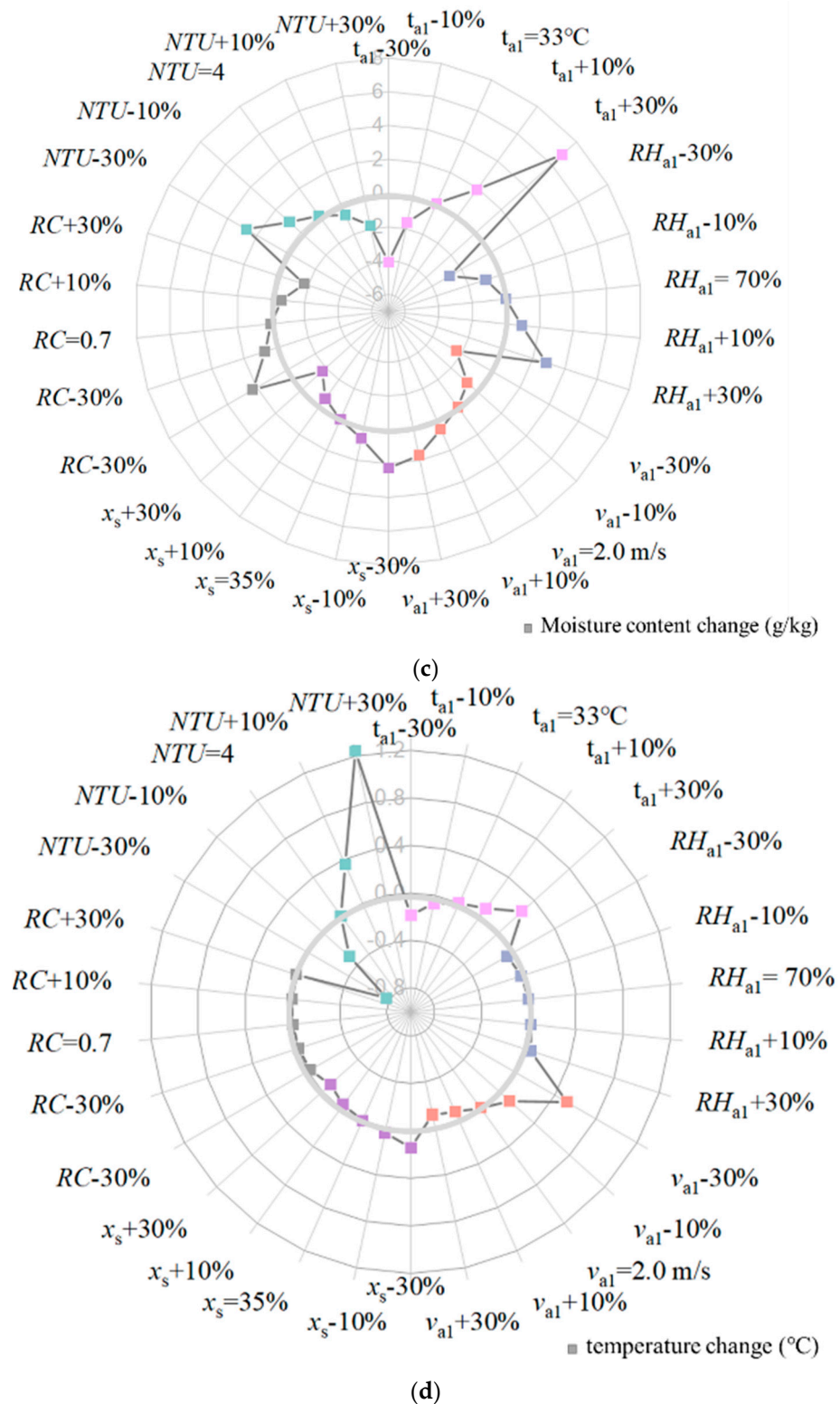


Figure 4. Influence of 6 sensitive factors. (a) COP of LDCS system under different parameters. (b) Influence of parameter variations on COP based on the baseline scenario. (c) Influence of parameter variations on outlet air moisture content change of the system based on the baseline scenario. (d) Influence of parameter variations on the change in outlet air temperature change based on the baseline scenario.

When the solution concentration was increased by 30%, the water vapor removal rate exhibited a significant increase of 2.281 g/kg. Surprisingly, the system outlet temperature

did not experience a substantial rise, with only a marginal increase of $0.14\text{ }^{\circ}\text{C}$ observed. This unexpected result can be attributed to the improved dehumidification capability of the higher-concentration solution. Although the high x_s released heat during the water absorption process, the enhanced dehumidification capacity led to a decrease in the wet-bulb temperature of the working air entering the *RIEC* system. This reduction in moisture content increased the potential for cooling, compensating for the heat released by the solution. Consequently, the overall temperature rise at the system outlet remained relatively small. Figure 4d also demonstrates that changing the six parameters significantly influences the temperature of the system outlet air. The number of transfer units (*NTU*), which represents the heat exchanger's geometry and heat transfer capacity, plays a crucial role. By selecting a heat exchanger with a 30% higher *NTU* value, the outlet air temperature can be reduced by $1.2\text{ }^{\circ}\text{C}$.

These findings emphasize the importance of carefully considering and optimizing the selected parameters to achieve the desired outcomes in terms of both temperature and moisture control in the system.

4.2.2. Cross-Factor Analysis

It is important to recognize that the weights or impacts of the influencing factors leading to specific outcomes are not equal. Therefore, identifying the high-weight factors and addressing them first can help achieve the desired results. Some system parameters have been found to have cross-influences on the *COP*, allowing for flexible simultaneous changes to effectively enhance system performance. The Pareto bar chart (Figure 5) on the left side (*y*-axis) displays the *T*-values of each operating parameter in the system, with the influencing factors arranged on the *x*-axis in descending order of frequency. The results indicate that single-value operating parameters have the greatest impact on the *COP*, with the following ranking: secondary to primary air mass flow ratio in *LDD* (*RC*) > inlet air velocity (v_{a1}) > concentration of the solution (x_s). When *RC* is increased, the *IEC* extracts less return air, allowing more product air to enter the indoor space for heat and humidity treatment, resulting in better dehumidification potential and a higher *COP*. The cross-influence factor between v_{a1} and *RC* also significantly affects the target value of *COP*. Despite the positive correlation between x_s and v_{a1} with the coefficient of performance (*COP*), the cross-term $x_s * v_{a1}$ exhibits a negative correlation with the system *COP*. This is due to the fact that although increasing v_{a1} can enhance the processed air volume and increasing x_s can improve water absorption, the enhancement of water absorption requires more time to ensure a sufficient water absorption process.

4.2.3. Cross-Impact of System Parameters

Figure 6 illustrates the cross-interactions between the operational parameters *RC* and x_s on the coefficient of performance. Due to the presence of the quadratic term of x_s in the empirical formula, both *RC* and x_s are positively correlated with *COP*, resulting in a curved surface. The optimal *COP* is achieved at high *RC* and high x_s values. For example, at ($t_{a1} = 32$, $RH_{a1} = 70$), the *COP* reaches 7.50. Furthermore, when *RC* is high, *COP* is more sensitive to improvements in x_s . In practical scenarios where the solubility of the solution may be limited, enhancing the secondary airflow volume of the *LDD* can also contribute to improvements in *COP*.

Figure 7 demonstrates the cross-interactions between *RC* and v_{a1} on *COP*. The results show that, without changing *RC*, increasing v_{a1} alone has a minimal impact on system *COP*. This can be attributed to the higher airflow volume requiring more energy consumption and potentially weakening the dehumidification effect. However, when both *RC* and v_{a1} are simultaneously increased, the system achieves a better *COP*. For instance, when both *RC* and v_{a1} are increased by 30%, the *COP* of the system improves from 5.66 to 7.82, resulting in a 38.1% increase.

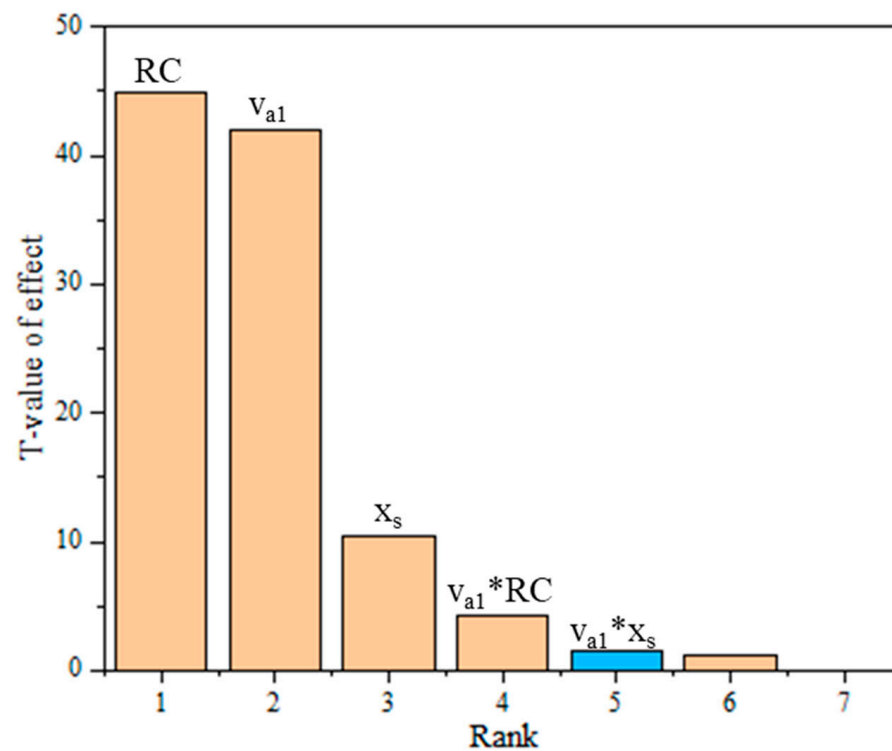


Figure 5. Pareto chart of the operating parameters and cross-influence factors. (RC: secondary to primary air mass flow ratio in LDD; v_{a1} : inlet air velocity; x_s : concentration of the solution; $v_{a1} * RC$: cross effect of the v_{a1} and RC; $v_{a1} * x_s$: cross effect of the v_{a1} and x_s).

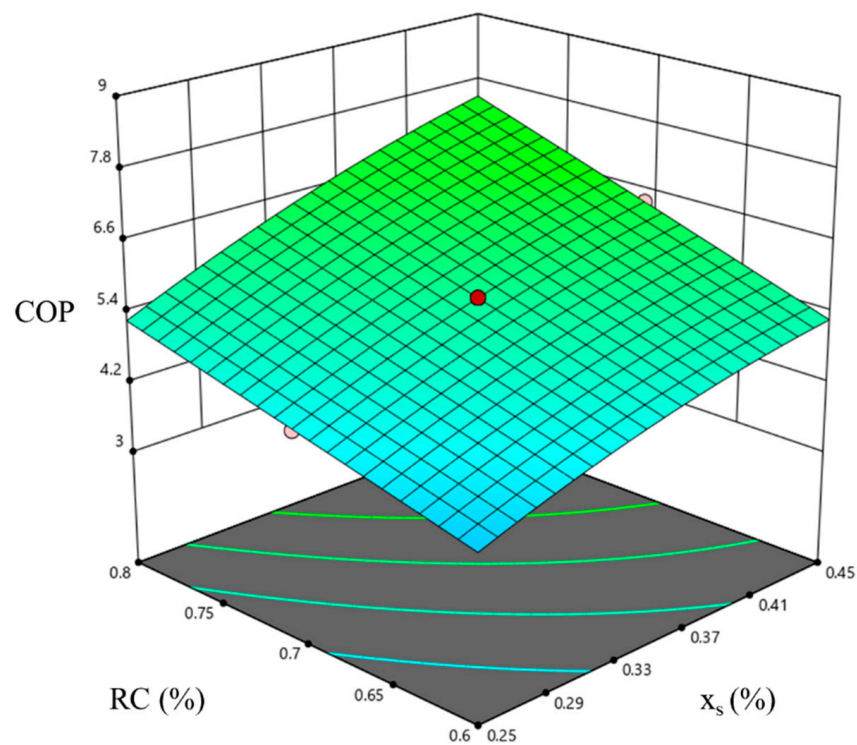


Figure 6. RSM model of cross-interactions between the operational parameters RC and x_s on the coefficient of performance.

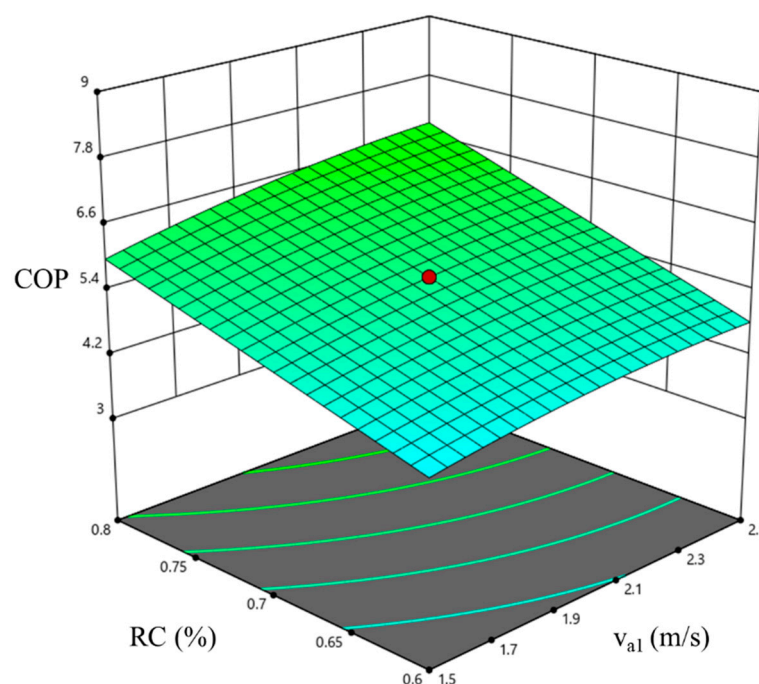


Figure 7. RSM model of cross-interactions between RC and v_{a1} (primary airflow velocity) on COP.

These findings highlight the importance of considering the combined effects of multiple parameters and their interactions when optimizing the COP of the LDCS system. By carefully adjusting RC, x_s , and v_{a1} , researchers and engineers can achieve significant improvements in the system performance and energy efficiency.

4.3. Regional Applicability of the LDCS System in Hot and Humid Regions

This section demonstrates the application of regression models for performance prediction in various hot and humid urban areas, alongside the implementation of optimized control strategies tailored to local meteorological conditions. Using derived regression models (Equations (20)–(22)), the operating parameters were optimized with outlet temperature and humidity content, as well as system COP as the optimization objectives (Table 3). The regional adaptability of the LDCS system was illustrated by operating it in three selected cities under the optimized parameters, as shown in Figures 8–10. The LDCS effectively reduced the outlet temperature and humidity during the high-temperature seasons in these regions, achieving performance coefficients (COP) ranging from 3.93 to 6.29, which is up to 57.25% increase compared to the MVCR system with a COP of 4.

In Kuala Lumpur, a city characterized by high temperatures and humidity year-round, maintaining high COPs (5.52–6.29) was achieved by setting optimized parameters ($v_{a1} = 2.3$ m/s, $x_s = 0.4$, RC = 0.75). Under this optimization strategy, the regression model predicted annual outlet temperature and humidity content in the ranges of 18.53–18.58 °C and 0.012–0.013 kg/kg, respectively. For San Juan, the optimized LDCS inlet air velocity was set at 2.3 m/s, balancing the airflow for cooling and dehumidification with RC set to 0.7. The outlet air temperature (t_{out}) ranged from 17.69–17.72 °C. In Hong Kong, the optimized system achieved a COP of 6.01 during the warmer months, although it varied throughout the year. The optimized system outperformed traditional evaporative vapor compression refrigeration systems (COP = 4) by 34.9% in terms of COP.

Given the year-round climate variations in hot and humid regions, further investigations may focus on operational modes to ensure the system's adaptability to different seasonal weather conditions.

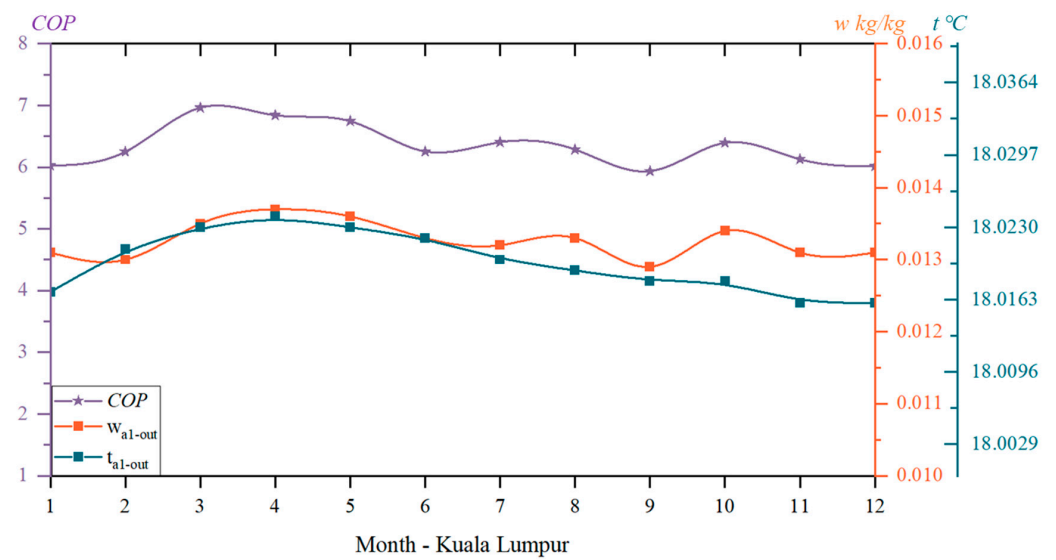


Figure 8. Optimized export temperature and humidity and COP Supplied in Kuala Lumpur.

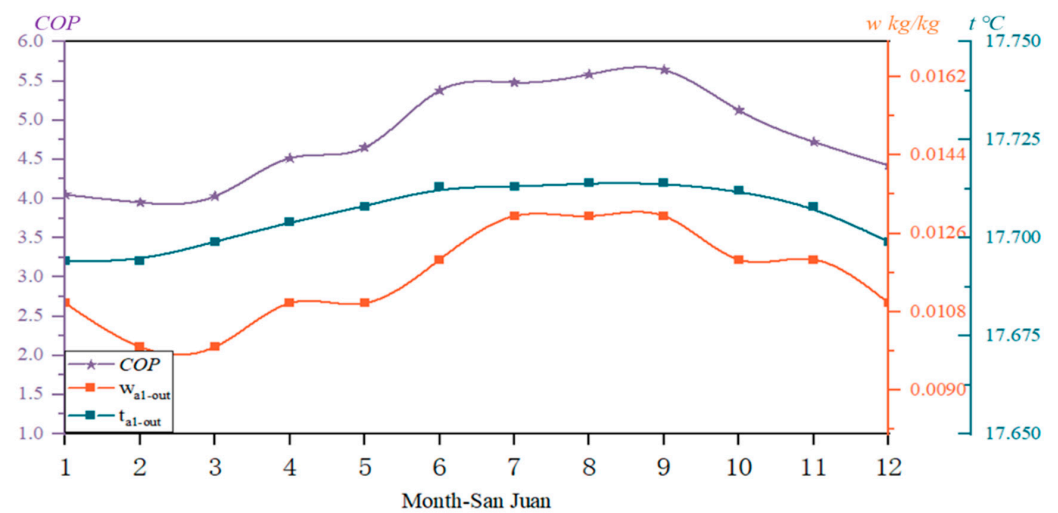


Figure 9. Optimized export temperature and humidity and COP plied in San Juan.

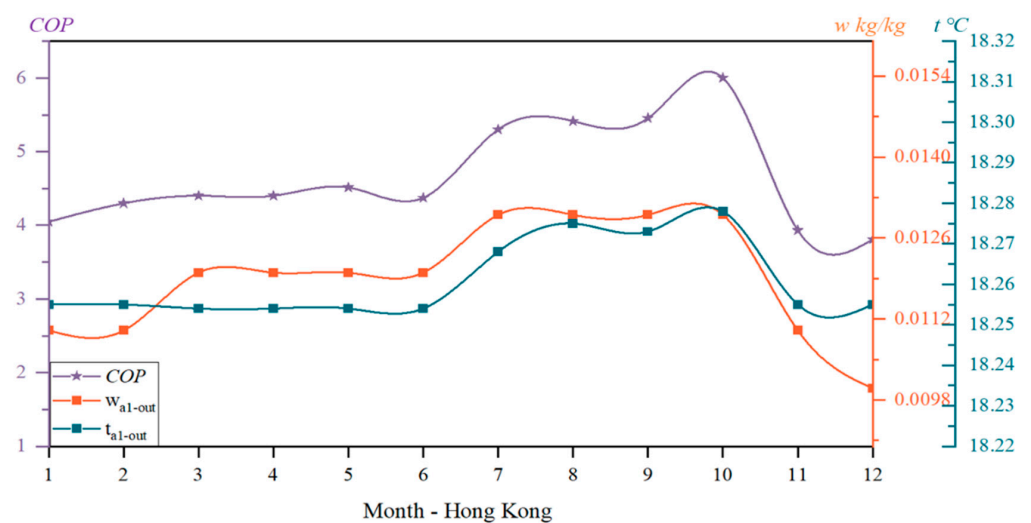


Figure 10. Optimized export temperature and humidity and COP applied in Hong Kong.

5. Conclusions

This study examined the performance of a regenerative liquid desiccant cooling system (*LDCS*) for dehumidification and cooling. Simulations from three cities were conducted, deriving empirical models to predict system performance. Sensitivity analysis and multi-objective optimization methods were employed to determine optimal system configurations.

The simulation results demonstrated that the secondary to primary air ratio of *LDD* (*RCD*) and airflow velocity (v_{a1}) having the most significant impact on system performance. The system maintained a high *COP* when operated under low airflow velocity ($v_{a1} = 1.5$ m/s) and high secondary to primary air ratio of *LDD* (*RCD* = 0.8) conditions.

The results of the dual-factor analysis of operating parameters indicated that when both *RCD* and v_{a1} were increased by 30%, the *COP* of the system improved from 5.66 to 7.82, representing a 38.1% enhancement. The optimal *COP* was achieved at high *RC* and high moisture removal (x_s) conditions, with a *COP* of 7.50 at a temperature of 32 °C and relative humidity of 70%.

The regional applicability results demonstrated that the *LDCS* has great potential for use in hot and humid regions, with a *COP* range of 3.93 to 6.29. The optimized *COP* was up to 57.25% higher than that of traditional evaporative cooling systems with mechanical vapor compression refrigeration (*MVCR*) systems.

This study contributes to the implementation of internally cooled *LDCS* and offers recommendations for their optimal operation in hot and humid regions. The regional applicability in diverse cities with varying weather conditions is investigated. This approach enables the control of the cooling and dehumidification process through the adjustment of operating parameters. Additionally, the optimized *COP* demonstrates a 57.25% improvement compared to the traditional evaporative cooling system with mechanical vapor compression refrigeration (*MVCR*).

Author Contributions: Conceptualization, Y.C.; Methodology, Y.Z.; Software, Y.Z.; Writing—original draft, Y.Z.; Writing—review & editing, H.Z. and Y.C.; Supervision, H.Y.; Project administration, Y.C. and C.W.L. All authors have read and agreed to the published version of the manuscript.

Funding: The work described in this paper was supported by grants from the Research Grants Council of Hong Kong (with grant numbers UGC/FDS24/E03/20 and UGC/IDS (24)/20).

Institutional Review Board Statement: Not applicable.

Informed Consent Statement: Not applicable.

Data Availability Statement: The data presented in this study are available on request from the corresponding author.

Conflicts of Interest: The authors declare no conflict of interest.

Nomenclatures

Symbols

A	Heat and mass transfer surface area per unit plate height	(m ² /m)
C	cooling capacity	kW
c_p	specific heat at constant pressure	(kJ/kg·K)
d	desirability function	
D	desirability value	
H	channel height	m
h	specific enthalpy	(kJ/kg)
K	heat transfer coefficient	(W/m ² ·K)
l	channel length	m
L	minimum response	
Le	lewis number	

m	mass flow rate	(kg/s)
n	number of desirability functions	
NTU	number of transfer units	
Q	heat exchange	(kW/m)
r	weight	
r_w	latent heat of vaporization	(kJ/kg)
R^2	coefficients of determination	
RC	secondary to primary air mass flow ratio in LDD	
re	secondary to primary air mass flow ratio in RIEC	
RH	relative humidity	%
T	maximum response	
t	temperature	(°C)
v	velocity	(m/s)
w	humidity ratio	(kg/kg)
x	x coordinate (fresh air flow direction)	
x_s	solution concentration	(%)
y	y coordinate (water flow direction)	
Greek symbols		
α	convection heat transfer coefficient	(W/m ² ·K)
α_m	mass transfer coefficient	(kg/m ² ·s)
η	dehumidification efficiency	%
ρ	density	(kg/m ³)
Subscripts		
a	air	
es	saturation	
ew	water and air interface	
g	dry air	
in	inlet	
lat	latent	
out	outlet	
s	solution	
sen	sensitive	
v	vapour	
w	water	
Abbreviation		
AC	air conditioning	
ANOVA	analysis of variance	
CCD	central composite design	
DFA	desirability function approach	
LDCS	liquid desiccant cooling system	
LDD	liquid desiccant dehumidification	
RIEC	regenerative indirect evaporative cooling	
RSM	response surface method	

References

1. Allison, C.K.; Stanton, N.A. Eco-driving: The role of feedback in reducing emissions from everyday driving behaviours. *Theor. Issues Ergon. Sci.* **2019**, *20*, 85–104. [[CrossRef](#)]
2. Liu, X.; Liu, X.; Jiang, Y.; Zhang, T.; Hao, B. Photovoltaics and Energy Storage Integrated Flexible Direct Current Distribution Systems of Buildings: Definition, Technology Review, and Application. *CSEE J. Power Energy Syst.* **2023**, *9*, 829–845. [[CrossRef](#)]
3. Census and Statistics Department. *Hong Kong Energy Statistics Annual Report*, 2021 Edition ed.; Census and Statistics Department: Wan Chai, Hong Kong, 2021.
4. Pérez-Lombard, L.; Ortiz, J.; Pout, C. A review on buildings energy consumption information. *Energy Build.* **2008**, *40*, 394–398. [[CrossRef](#)]
5. Guan, B.; Zhang, T.; Liu, J.; Liu, X.; Yin, Y. Review of internally cooled liquid desiccant air dehumidification: Materials, components, systems, and performances. *Build. Environ.* **2022**, *211*, 108747. [[CrossRef](#)]

6. Cuce, P.M.; Riffat, S. A state of the art review of evaporative cooling systems for building applications. *Renew. Sustain. Energy Rev.* **2016**, *54*, 1240–1249. [\[CrossRef\]](#)
7. Xuan, Y.M.; Xiao, F.; Niu, X.F.; Huang, X.; Wang, S.W. Research and application of evaporative cooling in China: A review (I)—Research. *Renew. Sustain. Energy Rev.* **2012**, *16*, 3535–3546. [\[CrossRef\]](#)
8. Chu, J.; Xu, W.; Fu, Y.; Huo, H. Experimental research on the cooling performance of a new regenerative dew point indirect evaporative cooler. *J. Build. Eng.* **2021**, *43*, 102921. [\[CrossRef\]](#)
9. Ren, Y.; Guo, C.; Lv, J.; Xu, J.; Dong, S.; Meng, D.; Ma, X.; Guo, S. Experimental study on a cross-flow energy recovered indirect evaporative cooling (ERIEC)-assisted liquid desiccant dehumidifier (LDD) with improved spraying nozzle and surface wetness. *Sci. Technol. Built Environ.* **2021**, *27*, 903–916. [\[CrossRef\]](#)
10. Zhang, H.; Ma, H.; Ma, S. Investigation on indirect evaporative cooling system integrated with liquid dehumidification. *Energy Build.* **2021**, *249*, 111179. [\[CrossRef\]](#)
11. Zhang, Y.; Zhang, H.; Yang, H.; Chen, Y.; Leung, C.W. Counter-crossflow indirect evaporative cooling-assisted liquid desiccant dehumidifier: Model development and parameter analysis. *Appl. Therm. Eng.* **2022**, *217*, 119231. [\[CrossRef\]](#)
12. Karami, M.; Delfani, S.; Noroozi, A. Performance characteristics of a solar desiccant/M-cycle air-conditioning system for the buildings in hot and humid areas. *Asian J. Civ. Eng.* **2020**, *21*, 189–199. [\[CrossRef\]](#)
13. Liu, X.; Xie, Y.; Zhang, T.; Chen, L.; Cong, L. Experimental investigation of a counter-flow heat pump driven liquid desiccant dehumidification system. *Energy Build.* **2018**, *179*, 223–238. [\[CrossRef\]](#)
14. Duan, Z.; Zhan, C.; Zhang, X.; Mustafa, M.; Zhao, X.; Alimohammadisagvand, B.; Hasan, A. Indirect evaporative cooling: Past, present and future potentials. *Renew. Sustain. Energy Rev.* **2012**, *16*, 6823–6850. [\[CrossRef\]](#)
15. Cho, H.-J.; Jeong, J.-W. Evaluation of thermal comfort in an office building served by a liquid desiccant-assisted evaporative cooling air-conditioning system. *Energy Build.* **2018**, *172*, 361–370. [\[CrossRef\]](#)
16. Kim, M.-H.; Park, J.-S.; Jeong, J.-W. Energy saving potential of liquid desiccant in evaporative-cooling-assisted 100% outdoor air system. *Energy* **2013**, *59*, 726–736. [\[CrossRef\]](#)
17. Kozubal, E.; Woods, J.; Burch, J.; Boranian, A.; Merrigan, T. *Desiccant Enhanced Evaporative Air-Conditioning (DEVap): Evaluation of a New Concept in Ultra Efficient Air Conditioning*; National Renewable Energy Lab. (NREL): Golden, CO, USA, 2011.
18. Heidarinejad, G.; Pasdarsahri, H. Potential of a desiccant-evaporative cooling system performance in a multi-climate country. *Int. J. Refrig.* **2011**, *34*, 1251–1261. [\[CrossRef\]](#)
19. Ren, H.; Ma, Z.; Li, W.; Tyagi, V.; Pandey, A. Optimisation of a renewable cooling and heating system using an integer-based genetic algorithm, response surface method and life cycle analysis. *Energy Convers. Manag.* **2021**, *230*, 113797. [\[CrossRef\]](#)
20. Hu, Y. Simulation Research on Performance of Internal Cooling Dehumidifier in Solution Dehumidification System. Master's Thesis, Lanzhou Jiaotong University, Lanzhou, China, 2018.
21. Zhang, Y.; Zhang, H.; Yang, H.; Chen, Y.; Leung, C.W. Response surface modeling and optimization scheme of an internally cooled liquid desiccant air conditioning system. *J. Build. Eng.* **2023**, *76*, 107371. [\[CrossRef\]](#)
22. Eltaweel, M.; Heggy, A.H.; Yaseen, Z.M.; Alawi, O.A.; Falah, M.W.; Hussein, O.A.; Ahmed, W.; Homod, R.Z.; Abdelrazek, A.H. Application of the ANOVA method in the optimization of a thermoelectric cooler-based dehumidification system. *Energy Rep.* **2022**, *8*, 10533–10545. [\[CrossRef\]](#)
23. Zhu, A.; Ali, H.; Ishaq, M.; Junaid, M.S.; Raza, J.; Amjad, M. Numerical Study of Heat and Mass Transfer for Williamson Nanofluid over Stretching/Shrinking Sheet along with Brownian and Thermophoresis Effects. *Energies* **2022**, *15*, 5926. [\[CrossRef\]](#)
24. Saman, W.Y.; Alizadeh, S. Modelling and performance analysis of a cross-flow type plate heat exchanger for dehumidification/cooling. *Sol. Energy* **2001**, *70*, 11. [\[CrossRef\]](#)
25. Riagvilaikul, B.; Kumar, S. An experimental study of a novel dew point evaporative cooling system. *Energy Build.* **2010**, *42*, 637–644. [\[CrossRef\]](#)
26. Conde, M.R. Properties of aqueous solutions of lithium and calcium chlorides: Formulations for use in air conditioning equipment design. *Int. J. Therm. Sci.* **2004**, *43*, 367–382. [\[CrossRef\]](#)
27. Qian, X.; Yang, Y.; Lee, S.W.; Caballes, M.J.; Alamu, O.S. Cooling performance analysis of the lab-scale hybrid oyster refrigeration system. *Processes* **2020**, *8*, 899. [\[CrossRef\]](#)
28. ASHRAE. 2005 ASHRAE Handbook: Fundamentals; ASHRAE: New York, NY, USA, 2005.

Disclaimer/Publisher's Note: The statements, opinions and data contained in all publications are solely those of the individual author(s) and contributor(s) and not of MDPI and/or the editor(s). MDPI and/or the editor(s) disclaim responsibility for any injury to people or property resulting from any ideas, methods, instructions or products referred to in the content.